Crystal plasticity forming limit diagram analysis of rolled aluminum sheets

Wu, P.D.; Neale, K.W.; van der Giessen, E.; Jain, M.; Makinde, A.; MacEwen, S.R.

Published in:
Metallurgical and Materials Transactions A-Physical Metallurgy and Materials Science

DOI:
10.1007/s11661-998-0134-x

Publication date:
1998

Crystal Plasticity Forming Limit Diagram Analysis of Rolled Aluminum Sheets

P.D. WU, K.W. NEALE, E. VAN DER GIESSEN, M. JAIN, A. MAKINDE, and S.R. MACEWEN

Numerical simulations of forming limit diagrams (FLDs) are performed based on a rate-sensitive polycrystal plasticity model together with the Marciniak–Kuczynski (M–K) approach. Sheet necking is initiated from an initial imperfection in terms of a narrow band. The deformations inside and outside the band are assumed to be homogeneous, and conditions of compatibility and equilibrium are enforced across the band interfaces. Thus, the polycrystal model needs only to be applied to two polycrystalline aggregates, one inside and one outside the band. Each grain is modeled as an fcc crystal with 12 distinct slip systems. The response of an aggregate comprised of many grains is based on an elastic-viscoplastic Taylor-type polycrystal model. With this formulation, the effects of initial imperfection intensity and orientation, initial distribution of grain orientations, crystal elasticity, strain-rate sensitivity, single slip hardening, and latent hardening on the FLD can be assessed. The predicted FLDs are compared with experimental data for the following rolled aluminum alloy sheets: AA5754-0-A, AA5754-0-B, AA6111-T4-A, AA6111-T4-C, and AA6111-T4-D.

I. INTRODUCTION

PLASTIC flow localization during sheet stretching limits metal formability. A sheet metal necks and localizes progressively until it fails when critical limit strains are approached. Forming limit diagrams (FLDs), which define maximum allowable strain levels during sheet metal forming, have become a standard tool for assessing and representing the formability of sheet metals.

Most theoretical and numerical studies on FLD analysis have been based on the so-called M–K approach developed by Marciniak and Kuczynski.[1] The basic assumption of this approach is the existence of material imperfections in the form of grooves on the surface of the sheet. They showed that the presence of even slight intrinsic inhomogeneities in load bearing capacity throughout a deforming sheet can lead to unstable growth of strain in the weaker regions, and subsequently cause localized necking and failure. Within the M–K framework, the influence of various constitutive features on FLDs has been explored using phenomenological plasticity models.[2,3] It is now well known that the FLD is very sensitive to, among others, effects of yield surface vertices, anisotropy, and material rate sensitivity.[4,5,6] For instance, a slight change of shape of the yield surface for a sheet metal can result in a large variation of its FLD.[7] Since the mechanical properties of a sheet metal are determined by its microstructure and microscopic properties, the FLD based on phenomenological models remains a diagnostic tool rather than a predictive one, because phenomenological models do not account for the effect of microstructure and its evolution with deformation. Crystallographic texture is usually the prime feature of microstructural evolution in sheet metals. To incorporate this, a crystal plasticity FLD analysis is required.

Bassani *et al.*[6] and Barlat and co-workers[8,9,10] calculated a series of Bishop and Hill yield surfaces of polycrystals corresponding to various crystallographic textures. Using yield surface functions to represent the computed Bishop and Hill yield surfaces, they obtained FLDs that were in fair agreement with the corresponding experimental observations.[11] However, these authors have not considered the subsequent evolution of the yield surface during deformation nor the effect of elasticity. Zhou and Neale[12] and Toth *et al.*[24] have directly applied a crystal plasticity model in conjunction with the M–K approach to predict FLDs for annealed fcc sheet metals. The initial texture and its evolution were considered in their analyses. However, elasticity was neglected in their simulations and the imperfection groove was restricted to be normal to the direction of major principal stretch (in Zhou and Neale[12]). The effect of elasticity was considered by Qiu *et al.*,[13] but again, the influence of groove orientation was not assessed in their analysis. Using their elastic-viscoplastic Taylor-type polycrystal model, Asaro and Needleman,[14] and later Tvergaard and Needleman,[15] calculated forming limit strains, but only for equibiaxial stretching and in-plane plane strain stretching rather than for the full range of biaxial strain ratios.

Very recently, Wu *et al.*[16] directly used the Asaro and Needleman polycrystal plasticity model[14] in a nonlinear numerical solution to calculate the FLDs for fcc polycrystals. This approach is also based on the M–K approach, in that sheet necking is initiated from an initial imperfection represented in terms of a narrow band, with the deformations inside and outside the band being homogeneous.

P.D. WU, formerly Research Scientist with the Faculty of Applied Science, University of Sherbrooke, is Research Scientist with the Kingston Research and Development Centre, Alcan International Ltd., Kingston, ON, Canada K7L 5L9. K.W. NEALE, Professor, is with the Faculty of Applied Science, University of Sherbrooke, Sherbrooke, PQ, Canada J1K 2R1. E. VAN DER GIESSEN is Professor with the Laboratory for Engineering Mechanics, Delft University of Technology, 2628 CD Delft, The Netherlands. M. JAIN, Research Scientist, and S.R. MacEWEN, Principal Research Scientist, are with the Kingston Research and Development Centre, Alcan International Ltd. A. MAKINDE, formerly Research Scientist with the Kingston Research and Development Centre, Alcan International Ltd., is Research Scientist with GE Corporation R & D, Schenectady, NY 12301.

Manuscript submitted July 11, 1997.

Thus, the rather complex polycrystal model needs only to be applied to two separate stress-strain histories, one inside and one outside the band. The conditions of compatibility and equilibrium are enforced across the band interfaces. Each grain is modeled as an fcc crystal with 12 distinct slip systems. The response of an aggregate comprised of many grains is based on the elastic-viscoplastic Taylor-type polycrystal model of Asaro and Needleman.[14] Since the deformations are assumed to be uniform both inside and outside the band, the computational requirements are relatively modest. The influence of the various model parameters on the FLD has been assessed systematically by Wu *et al.*[16] They showed that the initial texture and its evolution, initial imperfection groove orientation, and elasticity have significant effects on the predicted FLDs. The agreement between the predictions and the experimental data for one example of a rolled aluminum alloy sheet was shown to be quite good.

In this article, this technique is applied further to study the formabilities of five different rolled aluminum alloy sheets, namely, AA5754-0-A, AA5754-0-B, AA6111-T4-A, AA6111-T4-C, and AA6111-T4-D. The predictions are compared with the corresponding experimental data obtained from hemispherical punch stretching tests.

The plan of the article is as follows. In Section II, we briefly recapitulate the constitutive model. The problem formulation and the method of solution are presented in Section III. The predicted results and their comparisons with the experimental data are given in Section IV. The conclusion is presented in Section V.

Tensors and vectors will be denoted by boldface letters. The tensor product is denoted by $\otimes$ and the following operation for second-order tensors applies ($\mathbf{a} = a_{ij}\mathbf{e}_i \otimes \mathbf{e}_j$, $\mathbf{b} = b_{ij}\mathbf{e}_i \otimes \mathbf{e}_j$, $\mathbf{e}_i$ being a Cartesian basis): $\mathbf{ab} = a_{ik}b_{kj}\mathbf{e}_i \otimes \mathbf{e}_j$, $\mathbf{a} \cdot \mathbf{b} = a_{ij}b_{ij}$, with proper extension to high-order tensors. Superscripts T and -1 denote the transpose and inverse of a second-order tensor, respectively. The trace is denoted by tr. Furthermore, the range of Greek indexes is 1 . . . 2, while Latin indexes run from 1 to 3.

II. CONSTITUTIVE MODEL

In this section, we briefly recapitulate the constitutive framework adopted throughout this article. For details, we refer to Asaro and Needleman.[14] In the rate-sensitive crystal plasticity model employed, the elastic constitutive equation for each crystal is specified by

$$\overset{\nabla}{\boldsymbol{\sigma}} = \boldsymbol{\mathcal{L}}\mathbf{D} - \dot{\boldsymbol{\sigma}}^0 - \boldsymbol{\sigma}\,\mathrm{tr}\,\mathbf{D} \qquad [1]$$

where $\overset{\nabla}{\boldsymbol{\sigma}}$ is the Jaumann rate of the Cauchy stress, $\mathbf{D}$ represents the strain-rate tensor, and $\boldsymbol{\mathcal{L}}$ is the tensor of elastic moduli. These moduli are based on the anisotropic elastic constants of the fcc crystal and thus exhibit the appropriate cubic symmetry. The term $\dot{\boldsymbol{\sigma}}^0$ is a viscoplastic type stress rate that is determined by the slip rates on the various slip systems in the crystal.

The slip rates are taken to be governed by the power-law expression

$$\dot{\gamma}_{(\alpha)} = \dot{\gamma}_0\ \mathrm{sgn}\ \tau_{(\alpha)} \left|\frac{\tau_{(\alpha)}}{g_{(\alpha)}}\right|^{1/m} \qquad [2]$$

where $\tau_{(\alpha)}$ is the resolved shear stress on slip system α (the parentheses in the subscripts (α) indicate that α is not a tensor index and ranges from 1 to the number of slip systems), $g_{(\alpha)}$ is its hardness, m is the strain-rate sensitivity index, and $\dot{\gamma}_0$ is the reference shear rate. The $g_{(\alpha)}$ characterize the current strain hardened state of all slip systems. For multiple slip, the evolution of the hardness is governed by

$$\dot{g}_{(\alpha)} = \sum_{\beta} h_{(\alpha\beta)}|\dot{\gamma}_{(\beta)}| \qquad [3]$$

where $g_{(\alpha)}(0)$ is the initial hardness and is taken to be a constant τ_0 for each slip system and where the $h_{(\alpha\beta)}$ values are the hardening moduli. The moduli are assumed to have the form

$$h_{(\alpha\beta)} = q_{(\alpha\beta)}h_{(\beta)} \quad (\text{no sum on } \beta) \qquad [4]$$

where $h_{(\beta)}$ is a single slip hardening rate and $q_{(\alpha\beta)}$ is the matrix describing the latent hardening behavior of the crystallite. The latter is determined by a latent hardening parameter $q \geq 1$, if $q = 1$, hardening is isotropic.

The single slip hardening law employed in this article takes the following power-law form of the constitutive function $h_{(\beta)}$:

$$h_{(\beta)} = h_0\left(\frac{h_0\gamma_\alpha}{\tau_0 n} + 1\right)^{n-1} \qquad [5]$$

where h_0 is the system's initial hardening rate, n is the hardening exponent and γ_α is the accumulated slip.

The response of a polycrystal comprised of many grains is obtained by invoking the Taylor assumption. Thus, at a material point representing a polycrystal of N grains, the deformation in each grain is taken to be identical to the macroscopic deformation of the continuum. Furthermore, the macroscopic values of all quantities such as stresses, stress rates, and elastic moduli are obtained by averaging their respective values over the total number of grains at the particular material point.

III. PROBLEM FORMULATION AND METHOD OF SOLUTION

The FLD analysis is applied to polycrystalline sheets having orthotropic textures. The axes x_1 and x_2 define the directions of orthotropy in the plane of the sheet, while x_3 represents the direction normal to the sheet. In the numerical simulations, textures satisfying these conditions of orthotropy will be employed.

We consider a sheet having a nonuniformity in the form of a groove or band that is initially inclined at an angle ψ_I with respect to the x_1 reference direction (Figure 1). Quantities inside the band are denoted by $(\,)^b$. The thickness along the minimum section in the band is denoted by $h^b(t)$, with an initial value $h^b(0)$. The initial geometric nonuniformity is defined by

$$f = \frac{h^b(0)}{h(0)} \qquad [6]$$

where $h(0)$ is the initial thickness outside the band.

The loading imposed on the edges of the sheet is assumed to be such that

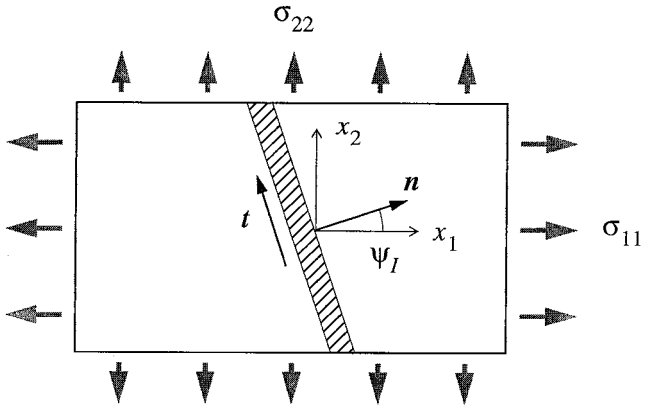

Fig. 1—Thin sheet with an initial thickness imperfection.

$$\frac{D_{22}}{D_{11}} = \frac{\dot{\varepsilon}_{22}}{\dot{\varepsilon}_{11}} = \rho = \text{const.}, \quad D_{12} = 0, \quad W_{12} = 0 \qquad [7]$$

where $\dot{\varepsilon}_{22} \equiv D_{22}$ and $\dot{\varepsilon}_{11} \equiv D_{11}$ are the (principal) logarithmic strain rates and the W_{ij} values are components of the spin tensor. We further assume that $D_{13} = D_{23} = W_{13} = W_{23} = 0$, while D_{33} is specified by the condition $\dot{\sigma}_{33} = 0$. For the orthotropic textures considered, these boundary conditions imply that the average stress components $\sigma_{13} = \sigma_{23} = 0$. Under this deformation model, the current groove orientation ψ is given by

$$\tan \psi = \exp [(1 - \rho)\varepsilon_{11}] \tan \psi_I \qquad [8]$$

Since uniform deformations are assumed both inside and outside the band, equilibrium and compatibility inside and outside the band are automatically satisfied, apart from the necessary conditions at the band interface. Following Hutchinson and Neale,[4] the compatibility condition at the band interface is given in terms of the differences in the velocity gradients inside and outside the band:

$$L^b_{\alpha\beta} = L_{\alpha\beta} + \dot{c}_\alpha n_\beta \qquad [9]$$

or

$$D^b_{\alpha\beta} = D_{\alpha\beta} + \frac{1}{2}(\dot{c}_\alpha n_\beta + n_\alpha \dot{c}_\beta), \quad W^b_{\alpha\beta} = W_{\alpha\beta} + \frac{1}{2}(\dot{c}_\alpha n_\beta - n_\alpha \dot{c}_\beta) \qquad [10]$$

Here, $n_1 = \cos \psi$ and $n_2 = \sin \psi$ are the components of the unit normal to the band in the current configuration and the $\dot{c}_\alpha$ values are the parameters to be determined. Equilibrium requires balance on each side of the interface,

$$n_\alpha \sigma^b_{\alpha\beta} h^b = n_\alpha \sigma_{\alpha\beta} h \qquad [11]$$

in the current configuration. Now, a set of incremental equations for $\dot{c}_\alpha$ are obtained by substituting the incremental constitutive relation [1] into the incremental form of Eq. [11], using Eq. [10] to eliminate the strain increments $D^b_{\alpha\beta}$. Together with the condition $\dot{\sigma}^b_{33} = 0$, this furnishes three algebraic equations for solving $\dot{c}_1$, $\dot{c}_2$, and the unknown D^b_{33}.

The solution is obtained numerically by a linear incremental procedure. At any given stage of the prescribed strain path, the moduli $\mathbf{L}$ and $\dot{\boldsymbol{\sigma}}^0$ in Eq. [1] are calculated for all grains inside and outside the band, by updating from the previous increment. The corresponding moduli and the viscoplastic type stress rates for the polycrystals representing materials inside and outside the band are obtained by averaging over all grains inside and outside the band, respectively. Therefore, the rates $\dot{c}_\alpha$, or $D^b_{\alpha\beta}$, and D^b_{33} inside the band are directly calculated by solving the three aforementioned algebraic equations. The sheet thicknesses outside the band h and inside the band h^b are updated based on the rates

$$\dot{h} = D_{33} h, \quad \dot{h}^b = D^b_{33} h^b \qquad [12]$$

For numerical stability, the polycrystal constitutive equations are implemented *via* the one-step, explicit rate-tangent method described by Peirce *et al.*[17] Moreover, an adaptive time-stepping method developed by Van der Giessen and Neale[18] is used. Finally, an equilibrium correction procedure is applied to prevent drifting of the solution from the true equilibrium path.

The onset of sheet necking is defined by the occurrence of a much higher maximum principal logarithmic strain rate inside the band than outside, taken here as the condition $\dot{\varepsilon}^b/D_{11} \geq 10^5$. The corresponding principal logarithmic strains ε^*_{11} and ε^*_{22} outside the band are the limit strains. For a real sheet material, numerous initial imperfections exist with different orientations, resulting from surface roughness[9] or from microvoids in the materials.[19] The most conservative estimate of a forming limit strain is obtained by calculating the limit strain for various values of the chosen initial groove orientation and selecting the minimum limit strain as the predicted forming limiting strain. The entire FLD of a sheet is determined by repeating the procedure for different strain paths outside the band as prescribed by the strain ratio ρ.

IV. RESULTS AND DISCUSSION

We have investigated the formabilities of the following rolled aluminum sheets: AA5754-0-A, AA5754-0-B, AA6111-T4-A, AA6111-T4-C, and AA6111-T4-D. Figure 2 shows their initial textures represented by the {111} stereographic pole figures. For all of these cases, about 400 grains are used to represent initial textures. We take the rolling direction (RD) to be aligned with the major strain direction (x_1).

In all simulations, the crystal elastic constants are taken to be $C_{11} = 206$ GPa, $C_{12} = 118$ GPa, and $C_{44} = 54$ GPa. The slip system reference plastic shearing rate is assumed to be $\dot{\gamma}_0 = 0.001\ \text{s}^{-1}$, while the slip rate sensitivity parameter $m = 0.002$. These values of the material parameters are typical for an aluminum alloy. Furthermore, we assume isotropic slip system hardening ($q = 1$) in all the simulations reported here.

The hardening parameters in the constitutive model are estimated by curve fitting numerical simulations of uniaxial tension (in the RD) to corresponding experimental data. The values of the hardening parameters found by this procedure are as follows:

AA5754-0-A: $\tau_0 = 22$ MPa, $h_0/\tau_0 = 182$, $n = 0.245$,
AA5754-0-B: $\tau_0 = 21$ MPa, $h_0/\tau_0 = 182$, $n = 0.245$,
AA6111-T4-A: $\tau_0 = 42$ MPa, $h_0/\tau_0 = 29$, $n = 0.24$,

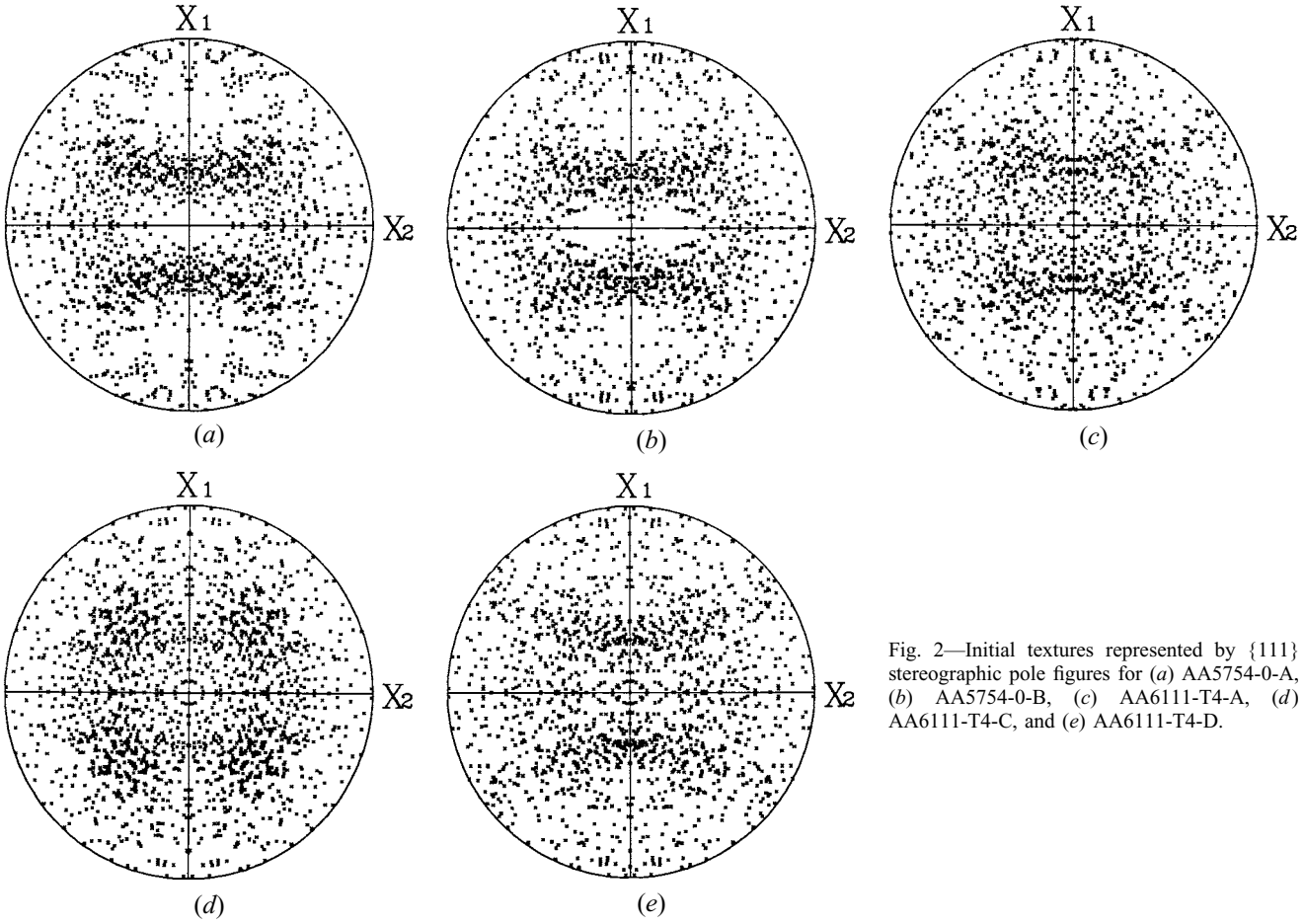

Fig. 2—Initial textures represented by {111} stereographic pole figures for (*a*) AA5754-0-A, (*b*) AA5754-0-B, (*c*) AA6111-T4-A, (*d*) AA6111-T4-C, and (*e*) AA6111-T4-D.

AA6111-T4-C: $\tau_0 = 47$ MPa, $h_0/\tau_0 = 30$, $n = 0.23$, and AA6111-T4-D: $\tau_0 = 46.5$ MPa, $h_0/\tau_0 = 30$, $n = 0.23$.

The correspondences between the calculated responses and the experimental stress-strain curves are presented in Figure 3. The curve fits are seen to be very good.

We proceed by numerically calculating the FLDs of the sheets, based on the crystal plasticity model together with the M–K approach, using the corresponding values of the material parameters determined previously. It is well known that the prediction of the FLD for elastic-viscoplastic materials, as considered in this article, relies on the gradual amplification of initial inhomogeneities. However, the value of the initial imperfection parameter f cannot be directly measured by physical experiments. The initial imperfection was assumed in Barlat and co-worker's study[20,21] to result from homogeneously distributed microcavities. Using a physical description of the cavities, they estimated an imperfection value of about 0.996 or 0.997. In this work, we have chosen the value of f for each sheet alloy by fitting the FLD prediction of in-plane plane strain tension ($\rho = 0$) to the corresponding experimental limit strain. Thus, we arrived at the following values of the initial imperfection parameter f: 0.996, 0.998, 0.996, 0.992, and 0.9985 for AA5754-0-A, AA5754-0-B, AA6111-T4-A, AA6111-T4-C, and AA6111-T4-D, respectively. For each material, these values are now used to predict the complete FLD.

Figures 4 through 8 show the predicted and measured FLDs. The general appearance of these figures is that the experimentally determined major limit strain ε_{11}^* decreases with ρ, almost linearly between uniaxial tension ($\rho = -0.5$) and in-plane plane strain tension ($\rho = 0$) to reach a minimum point, and then increases. With further increases in ρ, ε_{11}^* increases but eventually reaches a maximum and once again decreases. It is seen that the agreements between the simulated and the measured FLDs are quite good and that the shapes of the experimental FLDs are well predicted. Figure 4(b) shows the predicted critical groove orientations for AA5754-0-A. We scanned every 5 over the range of ψ_I's and then determined the critical groove angle that produces the minimum predicted localization strain. It was found that a groove oriented at $\psi_I = 0$ is favorable for necking when $0 \le \rho \le 0.7$. With increasing ρ from 0.7 to 1, the critical groove orientation increases from 0 to about 35 deg. In the region $-0.5 \le \rho \le 0$, the critical groove orientation decreases from 20 to 0 deg with increasing ρ. The trends for the predicted critical groove orientations for the other five sheet alloys are very similar to those shown in Figure 4(b).

The observed dip in the FLD near in-plane strain tension ($\rho = 0$) is rather significant for AA5754-0-B (Figure 5), AA6111-T4-A (Figure 6), and AA6111-T4-D (Figure 8), but is less so for AA5754-0-A (Figure 4) and AA6111-T4-C (Figure 7). This dip has also been observed experimentally by others,[22] but had not been predicted until very recently. Wu *et al.*[16] discussed the effect of crystal elasticity on the predicted FLDs. They pointed out that for a given initial texture, it is the elastic effect that determines the shape of the FLD near in-plane plane strain tension and

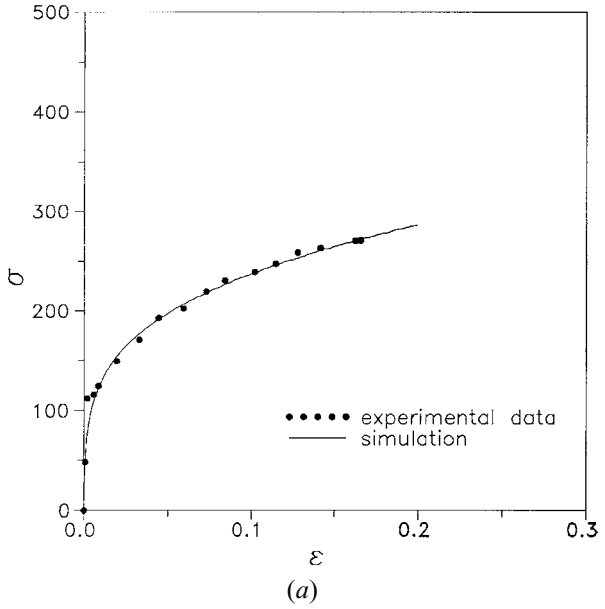

(*a*)

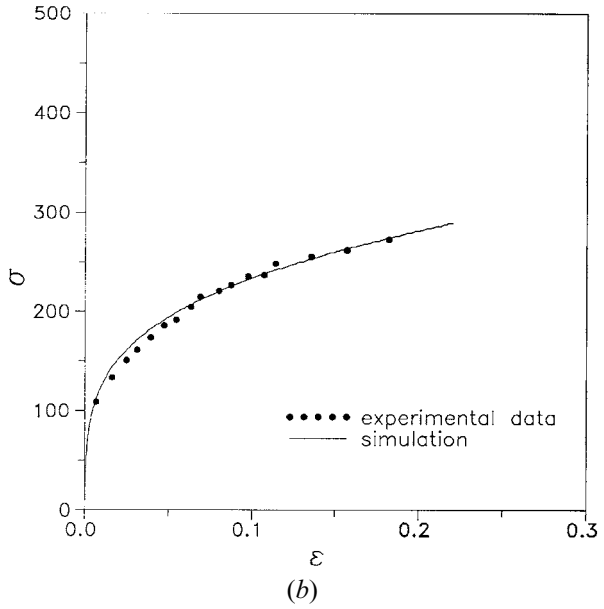

(*b*)

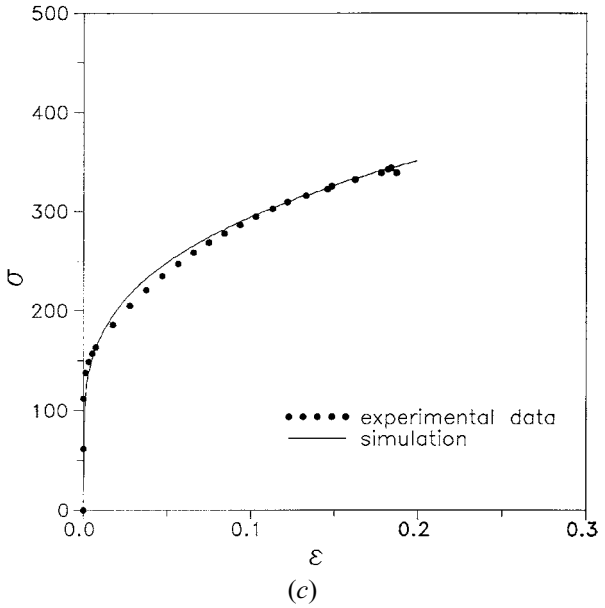

(*c*)

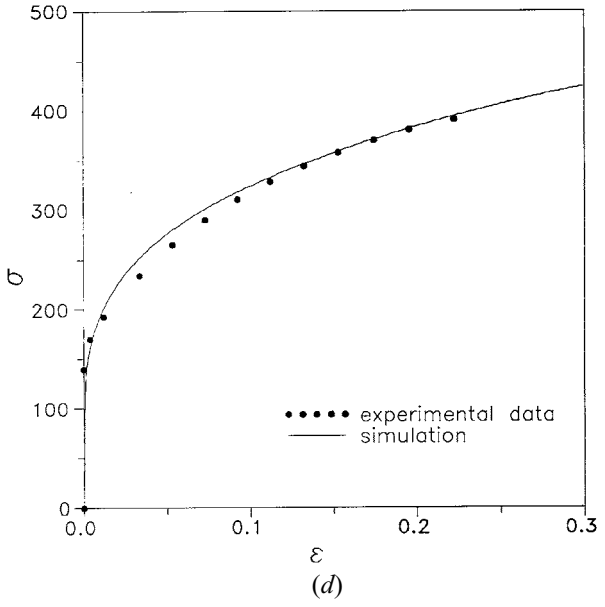

(*d*)

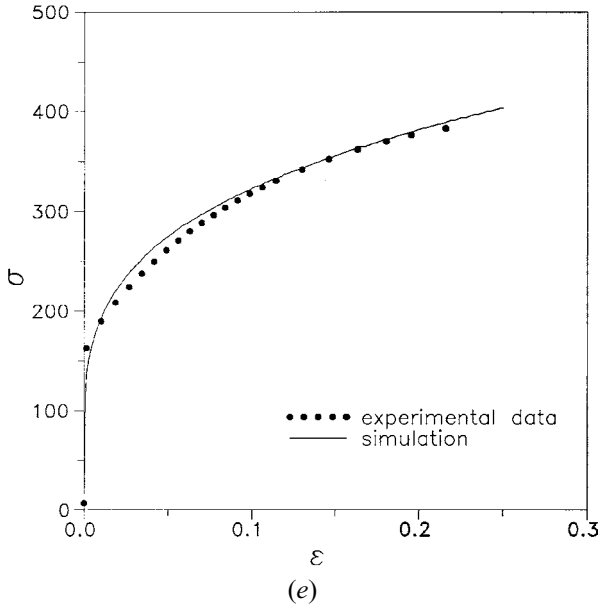

(*e*)

Fig. 3—Tensile stress-strain responses in uniaxial tension for (*a*) AA5754-0-A, (*b*) AA5754-0-B, (*c*) AA6111-T4-A, (*d*) AA6111-T4-C, and (*e*) AA6111-T4-D.

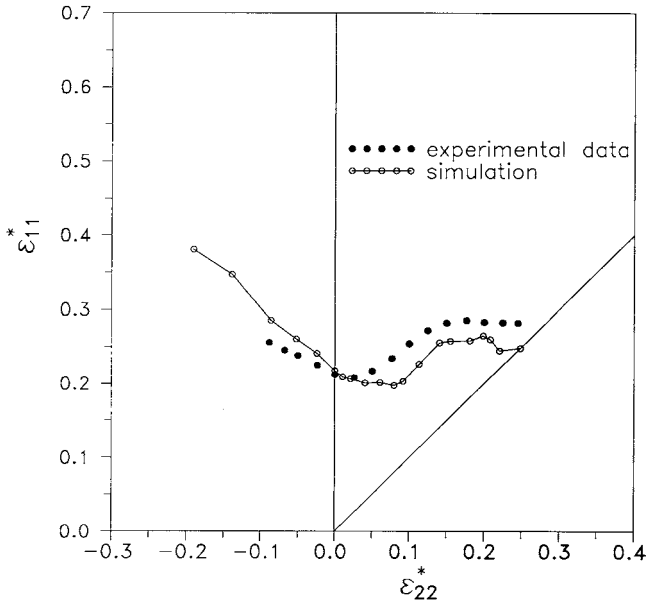

(a)

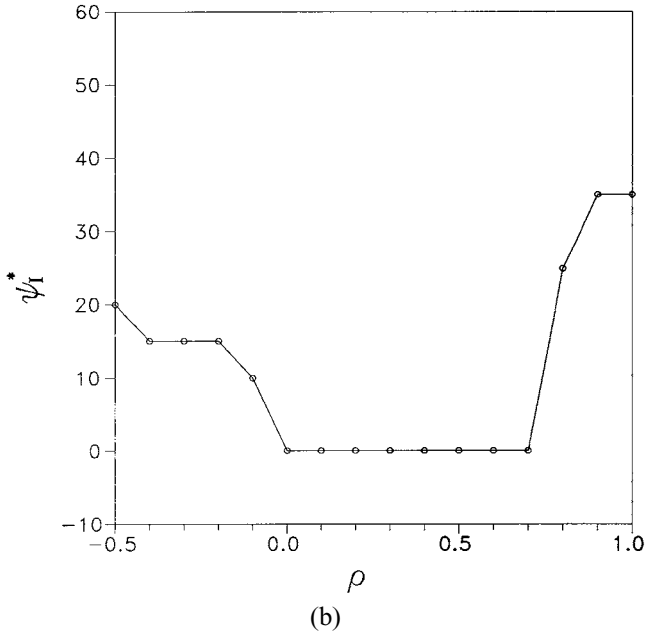

(b)

Fig. 4—Formability of AA5754-0-A: (*a*) FLDs and (*b*) the predicted critical groove orientations.

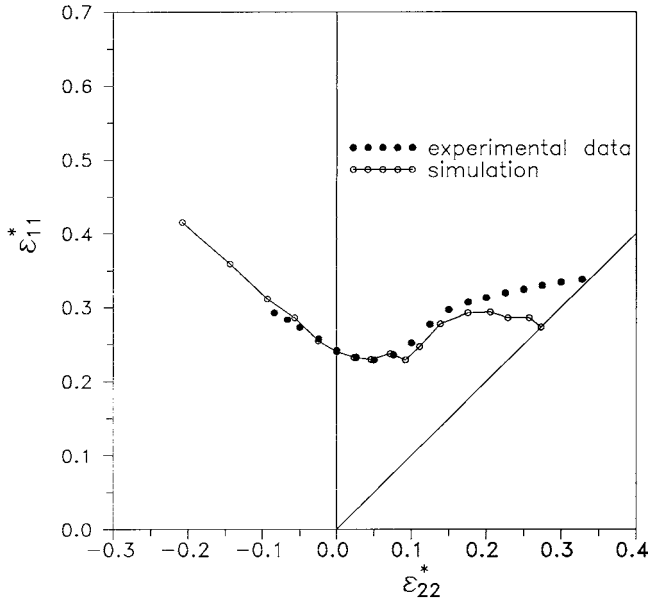

Fig. 5—Predicted and measured FLDs for AA5754-0-B.

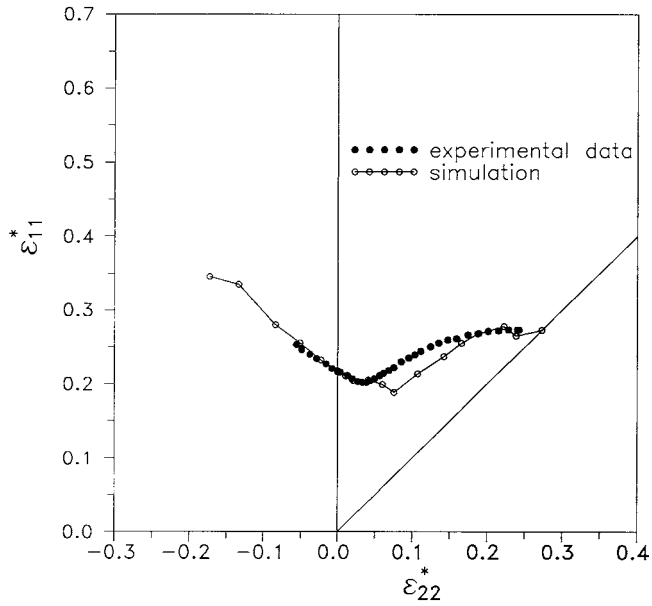

Fig. 6—Predicted and measured FLDs for AA6111-T4-A.

that ''rigid'' plasticity eliminates the dip in the FLD near in-plane plane strain tension. Their numerical simulations also indicated that increasing the elastic modulus of a sheet metal improves its formability.

It is well-known that the predicted FLD is very sensitive to effects of yield surface vertices and anisotropy; for instance, a slight change of the shape of the yield surface for a sheet metal can result in a large variation of its FLD.[7] In the crystal plasticity FLD analyses carried out here, the shape of the yield surface for a sheet metal is determined by the initial texture and its evolution. Consequently, the initial texture is one of the most important parameters affecting the FLD. It is noted that the differences in uniaxial tensile response between AA5754-0-A and AA5754-0-B and between AA6111-T4-C and AA6111-T4-D are very small (Figure 3). However, the differences in the corresponding FLDs are significant (Figures 4, 5, 7, and 8). These differences could be partially due to the different forming processes and heat treatments and must be partially due to the differences in the initial textures. Apparently, the effect of initial textures on FLDs needs to be further explored.

The influence of texture evolution on FLDs has already been shown to be important. Figure 9 gives the calculated textures at necking for AA6111-T4-A under in-plane plane strain tension. The texture outside the band at necking is a typical plane strain tension texture (Figure 9(a)). As expected, the texture inside the groove (Figure 9b) is stronger than that outside the groove. The simulated textures for the same sheet under balanced biaxial tension at necking are presented in Figure 10. Again, the texture outside the band

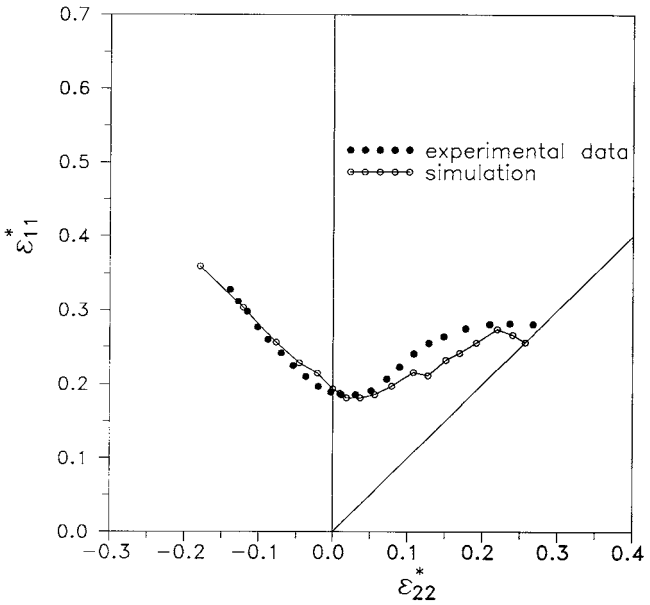

Fig. 7—Predicted and measured FLDs for AA6111-T4-C.

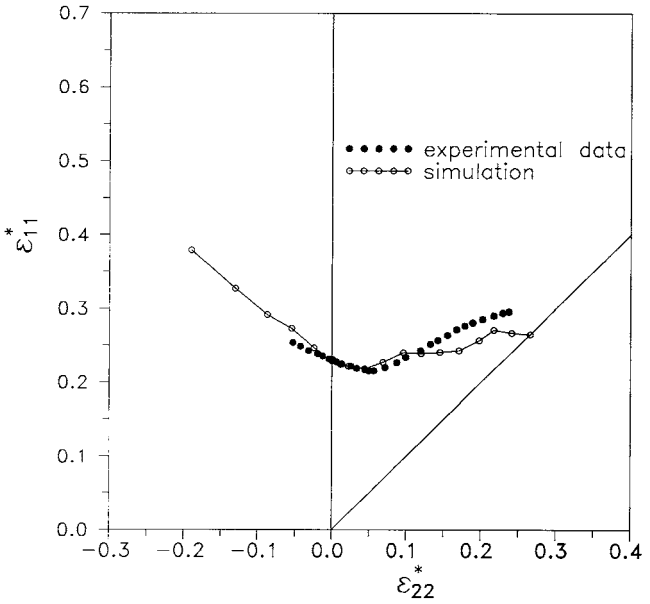

Fig. 8—Predicted and measured FLDs for AA6111-T4-D.

at necking follows the applied deformation and is a typical balanced biaxial tension texture (Figure 10(a)). The RD of the simulated texture inside the groove (Figure 10(b)) is found to be inclined at about 35 deg, since the critical groove orientation is, in this case, inclined at an angle ψ_I = 35 deg. Furthermore, the deformation-induced shear strain components inside the groove become noticeable. It is well known that the material inside the groove tends toward a plane strain deformation state irrespective of the deformation imposed outside the groove.[9] However, the simulated textures inside the groove (Figures 9(b) and 10(b)) only show a very weak plane strain tension texture, due to the fact that computations were stopped at the onset of necking (when $\dot{\bar{\varepsilon}}^b/D_{11} \geq 10^5$), and at that instant, the deformation inside the groove has not yet become very large as compared to the applied deformation. Figure 11

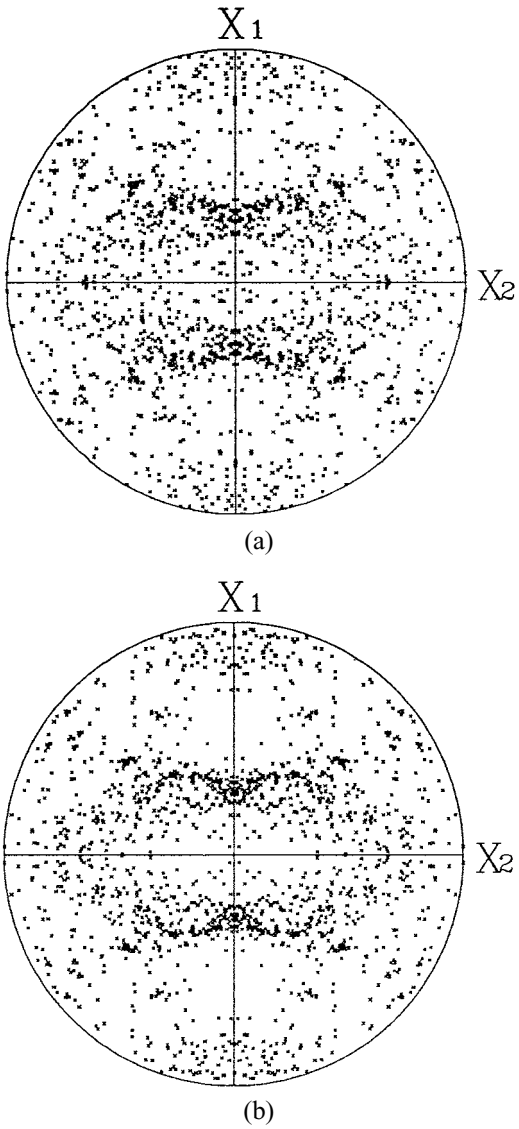

Fig. 9—Calculated textures at necking for AA6111-T4-A under in-plane plane strain tension (*a*) outside and (*b*) inside the groove.

shows the calculated textures at a point well beyond necking for AA6111-T4-A under the strain path ρ = 0.5. It is found that as the applied deformations concentrate completely in the groove after necking, the material inside the groove demonstrates texture development corresponding to a plane strain deformation state (Figure 11(b)).

One of the most important differences between the simulated and experimentally measured FLDs is that our simulations tend to underestimate the limit strains as ρ approaches equibiaxial stretching (ρ = 1). This could be due to the fact that we simulated in-plane stretching deformation processes, while the experimental data were obtained from hemispherical punch stretching tests. In punch tests, there are compressive stresses normal to the sheet, frictional shear stresses, and sheet curvature. Furthermore, proportional straining (constant ρ) is assumed in our calculations. This is not necessarily true for the punch stretching experiments. These complicating factors have not been accounted for in our analyses, while they are likely to have a stronger effect as the strains become larger. Furthermore, it should be noted in making these comparisons that it has

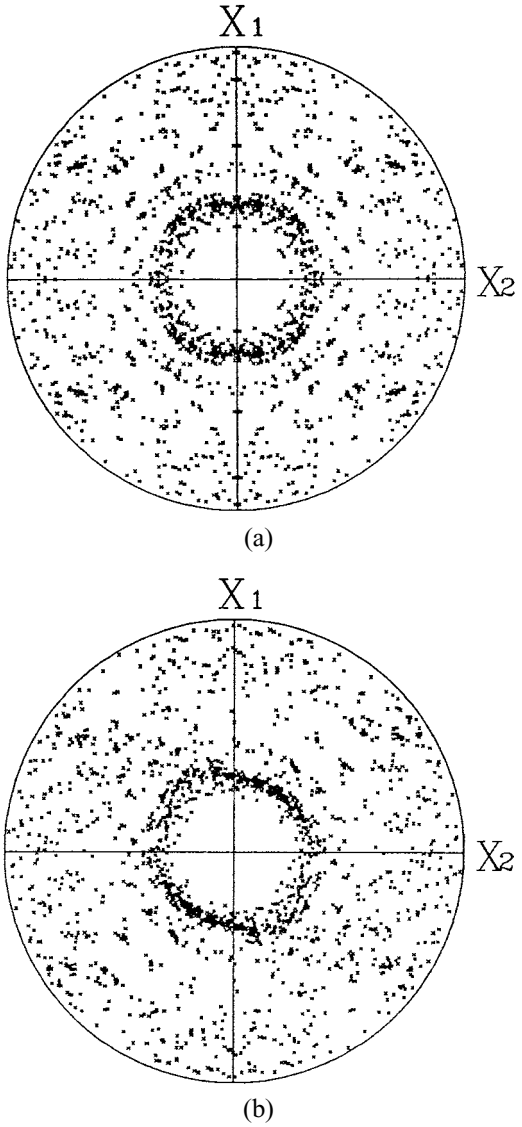

Fig. 10—Calculated textures at necking for AA6111-T4-A under balanced biaxial tension (*a*) outside and (*b*) inside the groove.

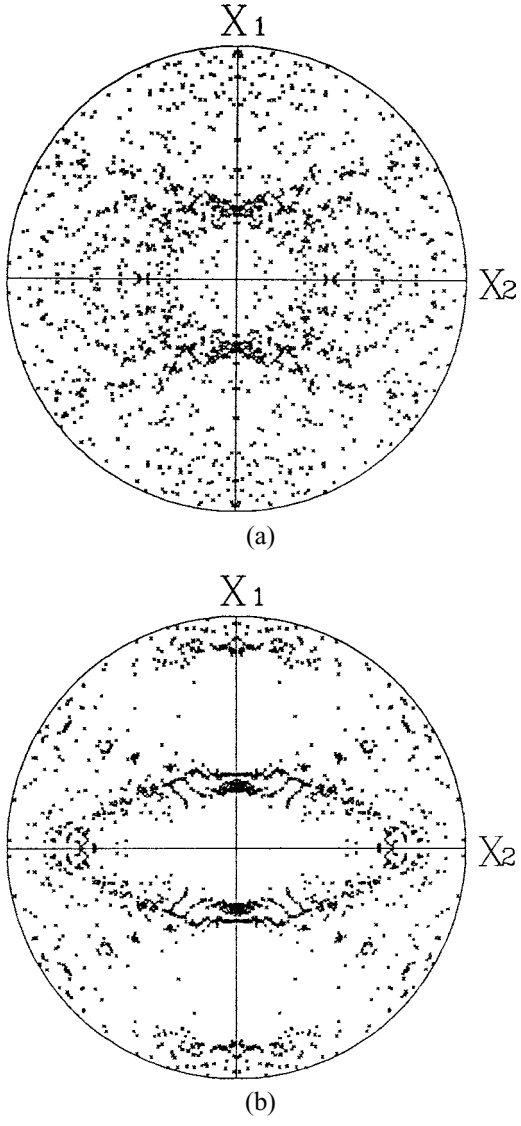

Fig. 11—Calculated textures at a point well beyond necking for AA6111-T4-A under biaxial tension $\rho = 0.5$ (*a*) outside and (*b*) inside the groove.

been found[23] that FLDs measured from in-plane stretching tend to lie below the corresponding punch-stretching FLDs.

V. CONCLUSIONS

In this article, we have predicted complete FLDs, using the elastic-viscoplastic Taylor-type polycrystal plasticity model developed by Asaro and Needleman,[14] for five aluminum alloy sheets: AA5754-0-A, AA5754-0-B, AA6111-T4-A, AA6111-T4-C, and AA6111-T4-D. The computations for each material are based on the initial texture measured experimentally and on material parameters determined using the uniaxial stress-strain curve. The effects of initial imperfection intensity and orientation, texture evolution, crystal elasticity, strain rate sensitivity, single slip hardening, and latent hardening on the FLD have been accounted for in the simulations. The predicted FLDs have been compared with experimental data obtained from standard hemispherical punch tests used in practice. The agreements between the simulated and measured FLDs are quite good. The characteristic shapes of the experimental FLDs are predicted well, but details of the FLDs may be somewhat different quantitatively.

ACKNOWLEDGMENTS

This work was supported by the Natural Sciences and Engineering Research Council of Canada (NSERC) and Alcan International Limited.

REFERENCES

1. Z. Marciniak and K. Kuczynski: *Int. J. Mech. Sci.*, 1967, vol. 9, pp. 609-20.
2. K.S. Chan: in *Forming Limit Diagrams: Concepts, Methods and Applications*, R.H. Wagoner, K.S. Chan, and S.P. Keeler, eds., TMS, Warrendale, PA, 1989, pp. 73-110.
3. G. Ferron and A. Molinari: in *Forming Limit Diagrams: Concepts, Methods and Applications*, R.H. Wagoner, K.S. Chan, and S.P. Keeler, eds., TMS, Warrendale, PA, 1989, pp. 111-51.
4. J.W. Hutchinson and K.W. Neale: in *Mechanics of Sheet Metal*

Forming, K.P. Koistinen and N.-M. Wang, eds., Plenum Press, New York, NY, 1978, pp. 269-85.
5. J.R. Rice and S. Stören: *J. Mech. Phys. Solids*, 1978, vol. 23, pp. 421-41.
6. J.L. Bassani, J.W. Hutchinson, and K.W. Neale: in *Metal Forming Plasticity*, H. Lippman, ed., Springer-Verlag, Berlin, 1979, pp. 1-13.
7. K.W. Neale and E. Chater: *Int. J. Mech. Sci.*, 1980, vol. 22, pp. 563-74.
8. F. Barlat: *Mater. Sci. Technol.*, 1987, vol. 91, pp. 55-72.
9. F. Barlat: in *Forming Limit Diagrams: Concepts, Methods and Applications*, R.H. Wagoner, K.S. Chan, and S.P. Keeler, eds., TMS, Warrendale, PA, 1989, pp. 275-301.
10. F. Barlat and O. Richmond: *Mater. Sci. Technol.*, 1987, vol. 95, pp. 15-29.
11. D.J. Lege, F. Barlat, and J.C. Brem: *Int. J. Mech. Sci.*, 1989, vol. 31, pp. 549-63.
12. Y. Zhou and K.W. Neale: *Int. J. Mech. Sci.*, 1995, vol. 37, pp. 1-20.
13. Y. Qiu, K.W. Neale, A. Makinde, and S.R. MacEwen: in *Simulation of Materials Processing: Theory, Methods and Applications*, S. Shen and P.R. Dawson, eds., Balkema, Rotterdam, 1995, pp. 327-31.
14. R.J. Asaro and A. Needleman: *Acta Metall.*, 1985, vol. 33, pp. 923-53.
15. V. Tvergaard and A. Needleman: *Proc. R. Soc. London*, 1993, vol. A443, pp. 547-62.
16. P.D. Wu, K.W. Neale, and E. van der Giessen: *Proc. R. Soc. London*, 1997, vol. A453, pp. 1831-1848.
17. D. Peirce, C.F. Shih, and A. Needleman: *Computers and Structures*, 1982, vol. 18, pp. 875-87.
18. E. Van der Giessen and K.W. Neale: *Comp. Meth. Appl. Mech. Eng.*, 1993, vol. 103, pp. 291-313.
19. D.V. Wilson, W.T. Roberts, and P.M.B. Rodrigues: *Metall. Trans. A*, 1981, vol. 12A, pp. 1595-1611.
20. F. Barlat, A. Barata da Roberts, and J.M. Jalinier: *J. Mater. Sci.*, 1984, vol. 19, pp. 4133-37.
21. F. Barlat and J.M. Jalinier: *J. Mater. Sci.*, 1985, vol. 20, pp. 3385-99.
22. P. Ratchev, P. Van Houtte, B. Verlinden, P. De Smet, P. Neutjens, R. Baartman, and P. Drent: *Text. Microstr.*, 1994, vol. 22, pp. 219-31.
23. A.K. Ghosh and S.S. Hecker: *Metall. Trans.*, 1974, vol. 5, pp. 2161-64.
24. L.S. Toth, J. Hirsch, and P. Van Houtte: *Int. J. Mech. Sci.*, 1996, vol. 38, pp. 1117-26.